HAL

archives-ouvertes.fr

All speed scheme for the low mach number limit of the Isentropic Euler equation

Pierre Degond, Min Tang

▶ To cite this version:

Pierre Degond, Min Tang. All speed scheme for the low mach number limit of the Isentropic Euler equation. 2009. <hal-00409851>

HAL Id: hal-00409851

https://hal.archives-ouvertes.fr/hal-00409851

Submitted on 13 Aug 2009

All speed scheme for the low mach number limit of the Isentropic Euler equation

Pierre Degond[1,2], Min Tang[1,2]

1-Université de Toulouse; UPS, INSA, UT1, UTM ;
Institut de Mathématiques de Toulouse ;
F-31062 Toulouse, France.
2-CNRS; Institut de Mathématiques de Toulouse UMR 5219 ;
F-31062 Toulouse, France.
email: pierre.degond@math.univ-toulouse.fr, tangmin1002@gmail.com

Abstract

An all speed scheme for the Isentropic Euler equation is presented in this paper. When the Mach number tends to zero, the compressible Euler equation converges to its incompressible counterpart, in which the density becomes a constant. Increasing approximation errors and severe stability constraints are the main difficulty in the low Mach regime. The key idea of our all speed scheme is the special semi-implicit time discretization, in which the low Mach number stiff term is divided into two parts, one being treated explicitly and the other one implicitly. Moreover, the flux of the density equation is also treated implicitly and an elliptic type equation is derived to obtain the density. In this way, the correct limit can be captured without requesting the mesh size and time step to be smaller than the Mach number. Compared with previous semi-implicit methods [11, 13, 27], non-physical oscillations can be suppressed. We develop this semi-implicit time discretization in the framework of a first order local Lax-Friedrich (LLF) scheme and numerical tests are displayed to demonstrate its performances.

AMS subject classification: 65M06,65Z05,76N99,76L05

Keywords: Low Mach number; isentropic euler equation; compressible flow; incompressible limit; asymptotic preserving; Lax-Friedrich scheme.

1

1 Introduction

Singular limit problems in fluid mechanics have drawn great attentions in the past years, like low-Mach number flows, magneto-hydrodynamics at small Mach and Alfven numbers and multiple-scale atmospheric flows. As mentioned in [17], the singular limit regime induces severe stiffness and stability problems for standard computational techniques. In this paper we focus on the simplest Isentropic Euler equation and propose a numerical scheme that is uniformly applicable and efficient for all ranges of Mach numbers.

The problem under study is the Isentropic Euler equation

$$\begin{cases} \partial_t \rho_\varepsilon + \nabla \cdot (\rho_\varepsilon \mathbf{u}_\varepsilon) = 0, \\ \partial_t (\rho_\varepsilon \mathbf{u}_\varepsilon) + \nabla \left(\rho_\varepsilon \mathbf{u}_\varepsilon \otimes \mathbf{u}_\varepsilon \right) + \frac{1}{\varepsilon^2} \nabla p_\varepsilon = 0. \end{cases} \tag{1}$$

where $\rho_\varepsilon, \rho_\varepsilon \mathbf{u}_\varepsilon$ is the density and momentum of the fluid respectively and ε is the scaled Mach number. This is one of the most studied nonlinear hyperbolic systems. For standard applications, the equation of state takes the form

$$p(\rho) = \Lambda \rho^\gamma, \tag{2}$$

where Λ, γ are constants depending on the physical problem.

It is rigorously proved by Klainerman and Majda [15, 16] that when $\varepsilon \to 0$, i.e. when the fluid velocity is small compared with the speed of sound [3], the solution of (1) converges to its incompressible counterpart. Formally, this can be obtained by inserting the expansion

$$\begin{aligned} \rho_\varepsilon &= \rho_0 + \varepsilon^2 \rho_{(2)} + \cdots, \\ \mathbf{u}_\varepsilon &= \mathbf{u}_0 + \varepsilon^2 \mathbf{u}_{(2)} + \cdots, \end{aligned} \tag{3}$$

into (1) and equate the same order of ε. The limit reads as follows [15, 18]:

$$\rho = \rho_0, \tag{4a}$$
$$\nabla \cdot \mathbf{u}_0 = 0, \tag{4b}$$
$$\partial_t \mathbf{u}_0 + \nabla (\mathbf{u}_0 \otimes \mathbf{u}_0) + \nabla p_0 = 0. \tag{4c}$$

Here p_0 is a scalar pressure that can be viewed as the Lagrange multiplier which enforces the incompressibility constraint. Physically, this limit means that in slow flows (compared with speed of sound), the factor $1/\varepsilon^2$ in the momentum equation in front of the pressure gradient generates fast pressure waves, which makes the pressure and therefore, the density, uniform in the domain [24, 23].

For atmosphere-ocean computing or fluid flows in engineering devices, when ε is small in (1), standard numerical methods become unacceptably expensive. Indeed, (1) has wave speeds of the form

$$\lambda = \mathbf{u}_\varepsilon \pm \frac{1}{\varepsilon} \sqrt{p'(\rho_\varepsilon)},$$

where $p'(\rho_\varepsilon)$ is the derivative with respect to ρ_ε. If a standard hyperbolic solver is used, the CFL requirement is $\Delta t = O(\varepsilon \Delta x)$. Moreover in order to maintain stability, the numerical dissipation required by the hyperbolic solver is proportional to $|\lambda|$. If $|\lambda| = O(\frac{1}{\varepsilon})$, in order to control the diffusion, we need to have $\Delta x = o(\varepsilon^r)$, where r is some appropriate constant. Thus the stability and accuracy highly depend on ε.

Our aim is to design a method whose stability and accuracy is independent of ε. The idea is to find an asymptotic preserving (AP) method, i.e. a method which gives a consistent discretization of the isentropic Euler equations (1) when $\Delta x, \Delta t$ resolve ε, and a consistent discretization of the incompressible limit (4) when $\varepsilon \to 0$ ($\Delta x, \Delta t$ being fixed). The efficiency of AP schemes at the low Mach number regime can be proved similarly as in [9]. The key idea of our all speed scheme is a specific semi-implicit time discretization, in which the low Mach number stiff term is divided into two parts, one part being treated explicitly and the other one implicitly. Moreover, the flux of the density equation is also treated implicitly. For the space discretization, when ε is $O(1)$, even if the initial condition is smooth, shocks will form due to the nonlinearity of the $\text{div}\big(\rho_\varepsilon \mathbf{u}_\varepsilon \otimes \mathbf{u}_\varepsilon\big)$ term and shock capturing methods should be employed here.

In the literature, lots of efforts have been made to find numerical schemes for the compressible equation that can also capture the zero Mach number limit [1, 6, 24, 23, 11]. In [1], Bijl and Wesseling split the pressure into thermodynamic and hydrodynamic pressure terms and solve them separately. Similar to this approach, the multiple pressure variable (MPV) method was proposed by Munz et al. in [24, 23]. There is also some recent work by J. Hauck, J-G. Liu and S. Jin [11]. Their approach involves specific splitting of the pressure term. We avoid using this splitting, the proper design of which seems very crucial in some cases.

Some similar ideas can be found in the ICE method, which is designed to adapt incompressible flow computation techniques using staggered meshes to the simulation compressible flows. The method was first introduced by Harlow and Amsdan in 1965 and 1971 [13,12] and is called Implicit Continuous-fluid Eulerian (ICE) technique. It is used to simulate single phase fluid dynamic problems with all flow speeds. They introduce two parameters in the continuity equation and the

momentum equation to combine information from both previous and forward time steps. However this method is not conservative, which leads to discrepancies in the shock speeds. Additionally it suffers from small wiggles when there are moving contact discontinuities. The first problem was solved by an iterative method, for example SIMPLE [25], or PISO [14]. In some recent work, Heul and Wesseling also find a conservative pressure-correction method [27]. All these methods are based on the so called MAC staggered mesh in order to be consistent with the staggered grid difference method for the incompressible Euler equations [13]. Specifically, if we write the simplified ICE technique presented in [2] in conservative form, we are led to the semi-discrete framework:

$$
\begin{cases}
\frac{\rho_\varepsilon^* - \rho_\varepsilon^n}{\Delta t} + \nabla \cdot (\rho_\varepsilon \mathbf{u}_\varepsilon)^n = 0, \\
\frac{(\rho_\varepsilon \mathbf{u}_\varepsilon)^* - (\rho_\varepsilon \mathbf{u}_\varepsilon)^n}{\Delta t} + \nabla(\rho_\varepsilon^n \mathbf{u}_\varepsilon^n \otimes \mathbf{u}_\varepsilon^n) = 0,
\end{cases}
\tag{5}
$$

$$
\begin{cases}
\frac{\rho_\varepsilon^{n+1} - \rho_\varepsilon^*}{\Delta t} + \nabla \cdot \left((\rho_\varepsilon \mathbf{u}_\varepsilon)^{n+1} - (\rho_\varepsilon \mathbf{u}_\varepsilon)^* \right) = 0, \\
\frac{(\rho_\varepsilon \mathbf{u}_\varepsilon)^{n+1} - (\rho_\varepsilon \mathbf{u}_\varepsilon)^*}{\Delta t} + \frac{1}{\varepsilon^2} \nabla p(\rho_\varepsilon^{n+1}) = 0.
\end{cases}
\tag{6}
$$

By substituting the gradient of the second equation of (6) into its first equation and using the results of the first equation (5), ρ_ε can be updated by solving an elliptic equation which does not degenerate when $\varepsilon \to 0$.

We use a similar idea in our method. However, we do not use the predictor-corrector procedure but we rather discretize the problem in a single step. We use standard shock capturing schemes which allows to guarantee the conservativity and the desired artificial viscosity. We only use implicit evaluations of the mass flux and pressure gradient terms to ensure stability and provide an extremely simple way to deal with the implicitness. Additionally, we propose a modification of the implicit treatment of the pressure equation. Indeed, using a similar idea as in [11], we split the pressure into two parts and put $\alpha p(\rho_\varepsilon)$ into the hyperbolic system. This makes the first system no longer be weakly hyperbolic and much more stable. The numerical results show the advantage of our method in the following sense:

- The method is in conservative form and can capture the right shock speeds.

- The non-physical oscillations [10] can be suppressed by choosing the proper value of the parameter which determines the fraction of implicitness used in the evaluation of the pressure gradient term. The choice of this parameter depends on the time and space step and on the specific problem.

In this paper we only use the first order LLF scheme. Higher order space and time discretizations will be subject of future work. The main objective of this work is to show that the semi-discrete time discretization provides a framework for developing AP methods for singular limit problems. Similar ideas can be extended to the full Euler equation and more complicated fluid model and have also been used in other contexts such as quasineutrality limits [4, 7] and magnetized fluids under stong magnetic fields [5].

The organization of this paper is as follows. Section 2 exposes the semi-implicit scheme and its capability to capture the incompressible limit is proved. The detailed one dimensional and two dimensional fully discretized schemes and their AP property are presented in section 3 and 4 respectively. In section 5, how to choose the ad-hoc parameter is discussed and finally, some numerical tests are given in section 6 to discuss the stability and accuracy of our scheme. The efficiency at both the compressible and low mach number regime are displayed. Finally, we conclude in section 6 with some discussion.

2 Time Semi-discrete scheme

Let Δt be the time step, $t^n = n\Delta t, n = 0, 1, \cdots$ and let the 'n' superscript denote the approximations at t^n. The semi-discrete scheme for the nth time step is

$$\frac{\rho_\varepsilon^{n+1} - \rho_\varepsilon^n}{\Delta t} + \nabla \cdot (\rho_\varepsilon \mathbf{u}_\varepsilon)^{n+1} = 0, \tag{7}$$

$$\frac{(\rho_\varepsilon \mathbf{u}_\varepsilon)^{n+1} - (\rho_\varepsilon \mathbf{u}_\varepsilon)^n}{\Delta t} + \text{div}\left(\rho_\varepsilon^n \mathbf{u}_\varepsilon^n \otimes \mathbf{u}_\varepsilon^n + \alpha p(\rho_\varepsilon^n)\right) + \frac{1 - \alpha\varepsilon^2}{\varepsilon^2}\nabla p(\rho_\varepsilon^{n+1})$$
$$= 0, \tag{8}$$

where α is an ad-hoc parameter which satisfies $\alpha \leq 1/\varepsilon^2$. The choice of α depends on the space and time steps and on the fluid speed. When the shock is strong, α should be bigger, which means that the system should be more explicit to follow the discontinuity more closely. We discuss the choice of α for specific equations of state in this paper and test its effect numerically. It depends on the required accuracy, the small parameter ε and the shock amplitude in a sometimes quite complex way.

Rewriting the momentum equation (8) as

$$(\rho_\varepsilon \mathbf{u}_\varepsilon)^{n+1} = (\rho_\varepsilon \mathbf{u}_\varepsilon)^n - \Delta t \nabla \left(\rho_\varepsilon^n \mathbf{u}_\varepsilon^n \otimes \mathbf{u}_\varepsilon^n + \alpha p(\rho_\varepsilon^n)\right) - \Delta t \frac{1 - \alpha\varepsilon^2}{\varepsilon^2}\nabla P(\rho_\varepsilon^{n+1})$$

5

and substituting it into the density equation, one gets

$$\rho_\varepsilon^{n+1} - \Delta t^2 \frac{1-\alpha\varepsilon^2}{\varepsilon^2} \Delta P(\rho_\varepsilon^{n+1}) = \phi(\rho_\varepsilon^n, \mathbf{u}_\varepsilon^n) \tag{9}$$

which is an elliptic equation that can be solved relatively easily. Here

$$\phi(\rho_\varepsilon^n, \mathbf{u}_\varepsilon^n) = \rho_\varepsilon^n - \Delta t \nabla \cdot (\rho_\varepsilon^n \mathbf{u}_\varepsilon^n) + \Delta t^2 \nabla \cdot \nabla (\rho_\varepsilon^n \mathbf{u}_\varepsilon^n \otimes \mathbf{u}_\varepsilon^n + \alpha p(\rho_\varepsilon^n)). \tag{10}$$

The Laplace operator in (9) can be approximated by $\nabla(P'(\rho_\varepsilon^n)\nabla\rho_\varepsilon^{n+1})$ and (9) becomes

$$\rho_\varepsilon^{n+1} - \Delta t^2 \frac{1-\alpha\varepsilon^2}{\varepsilon^2} \nabla \cdot (P'(\rho_\varepsilon^n)\nabla\rho_\varepsilon^{n+1}) = \phi(\rho_\varepsilon^n, \mathbf{u}_\varepsilon^n), \tag{11}$$

Though shocks will form for the original system (7)(8), we always add some numerical diffusion terms so that $\phi(\rho_\varepsilon^n, \mathbf{u}_\varepsilon^n)$ is smooth. Then so is ρ_ε^{n+1}. When we implement this method, ρ_ε^{n+1} can be obtained from (9) first and $\mathbf{u}_\varepsilon^n$ is then updated by the momentum equation (8) afterwards. Therefore, apart from the resolution of the elliptic equation (11), the scheme only involves explicit steps.

We now show that the scheme (7)(8) is asymptotic preserving. We introduce the formal expansion

$$\begin{aligned}
\rho_\varepsilon^n(x) &= \rho_{0c}^n + \varepsilon\rho_{(1)}^n(x) + \varepsilon^2\rho_{(2)}^n(x) + \cdots, \\
\mathbf{u}_\varepsilon^n &= \mathbf{u}_0^n(x) + \varepsilon\mathbf{u}_{(1)}^n(x) + \cdots.
\end{aligned} \tag{12}$$

In the sequel, the 'c' in the index means that the quantity is independent of space. When Δx, Δt are fixed and ε goes to 0 in (9), we formally have $\Delta P(\rho_0^{n+1}) = 0$, which implies that ρ_0^{n+1} is independent of space, where ρ_0^{n+1} is the limit of ρ_ε^{n+1} when $\varepsilon \to 0$. Thus we have

$$\frac{\rho_{0c}^{n+1} - \rho_{0c}^n}{\Delta t} + \nabla \cdot (\rho_{0c}\mathbf{u}_0)^{n+1} = 0 \tag{13}$$

by equating the $O(1)$ terms in the density equation (7). Integrating (13) over the computational domain, one gets

$$|\Omega|\frac{\rho_{0c}^{n+1} - \rho_{0c}^n}{\Delta t} = -\rho_{0c}^{n+1}\int_\Omega \nabla \cdot (\mathbf{u}_0)^{n+1} = -\rho_{0c}^{n+1}\int_{\partial\Omega} \mathbf{n} \cdot \mathbf{u}_0^{n+1}. \tag{14}$$

As discussed in [11], for wall boundary condition, periodic boundary condition and open boundary condition, (14) gives

$$\rho_{0c}^{n+1} = \rho_{0c}^n, \tag{15}$$

6

that is ρ_0 is also independent of time. Thus (13) also implies

$$\nabla \cdot \mathbf{u}_0^{n+1} = 0. \tag{16}$$

Then, by using the fact that the curl of the gradient of any scalar field is always zero, the curl of the $O(1)$ terms of the momentum equation (8) becomes

$$\nabla \times \frac{\mathbf{u}_0^{n+1} - \mathbf{u}_0^n}{\Delta t} + \nabla \times \nabla \left(\mathbf{u}_0^n \otimes \mathbf{u}_0^n \right) = 0. \tag{17}$$

Thus

$$\frac{\mathbf{u}_0^{n+1} - \mathbf{u}_0^n}{\Delta t} + \nabla \left(\mathbf{u}_0^n \otimes \mathbf{u}_0^n \right) + \nabla p_{(2)}^n = 0, \tag{18}$$

where $p_{(2)}^n$ is some scalar field.

Equations (15), (16), (18) are the semi-discretization in time of (4) and thus the scheme (7), (8) is consistent with the low Mach number limit $\varepsilon \to 0$ of the original compressible Euler equation. This statement is exactly saying that the scheme is AP. We can see that, in order to obtain the stability and AP properties, it is crucial to treat the flux in the density equation (7) implicitly.

Letting $U = (\rho_\varepsilon, \rho_\varepsilon \mathbf{u}_\varepsilon)^T$, we can write (7), (8) abstractly as

$$\frac{U^{n+1} - U^n}{\Delta t} + \nabla \cdot F(U^{n+\frac{1}{2}}) + QU^{n+1} = 0, \tag{19}$$

where

$$F(U^{n+1/2}) = \begin{pmatrix} (\rho_\varepsilon \mathbf{u}_\varepsilon)^{n+1} \\ \rho_\varepsilon^n \mathbf{u}_\varepsilon^n \otimes \mathbf{u}_\varepsilon^n + \alpha p(\rho_\varepsilon^n) \end{pmatrix}, \qquad Q = \begin{pmatrix} 0 & 0 \\ \frac{1 - \alpha \varepsilon^2}{\varepsilon^2} \nabla P & 0 \end{pmatrix}. \tag{20}$$

Here P is an operator on ρ_ε and $U^{n+1/2}$ reminds that the flux is partly implicit and partly explicit.

This semi-discretization gives us a framework for developing AP schemes that can capture the incompressible limit. Now we are left with the problem of how discretizing the space variable. Because shocks can form, considerable literature has been devoted to the design of high resolution methods that can capture the correct shock speed. Upwind schemes and central schemes are among the most widely used Godunov type schemes [19, 20, 21].

In the present paper, the hyperbolic operator

$$\frac{U^{n+1} - U^n}{\Delta t} + \nabla \cdot F(U^{n+\frac{1}{2}})$$

7

is approximated by an upwind hyperbolic solver and the stiff $1/\varepsilon^2$ factor in front of the pressure term is treated implicitly. The implicitness of the density flux is treated by combining it with the momentum equation. For simplicity, in the present work we only consider the first order modified Lax-Friedrich scheme with local evaluation of the wave-speed in the current and neighboring cell.

3   Full time and space discretization: One dimensional case

For simplicity, we consider the domain $\Omega = [0, 1]$. Using a uniform spatial mesh with $\Delta x = 1/M$, M being an positive integer, the grid points are defined as

$$x_j := j\Delta x, \qquad j = 0, 1, \cdots, M.$$

The flux and Jacobian matrix of (19) become

$$\tilde{F}(U) = \begin{pmatrix} \rho_\varepsilon \mathbf{u}_\varepsilon \\ \rho_\varepsilon \mathbf{u}_\varepsilon^2 + \alpha p(\rho_\varepsilon) \end{pmatrix}, \qquad \tilde{F}'(U) = \begin{pmatrix} 0 & 1 \\ -\mathbf{u}_\varepsilon^2 + \alpha p'(\rho_\varepsilon) & 2\mathbf{u}_\varepsilon \end{pmatrix}, \quad (21)$$

so, the wave speeds are
$$\lambda = \mathbf{u}_\varepsilon \pm \sqrt{\alpha p'(\rho_\varepsilon)}. \tag{22}$$

Let U_j be the approximation of $U(x_j)$ and let

$$A_{j+\frac{1}{2}}(t) = \max\left(|\lambda_j|, |\lambda_{j+1}|\right). \tag{23}$$

These are the local maximal wave-speeds in the current and neighboring cells. We discretize (19) in space as follows:

$$\frac{U_j^{n+1} - U_j^n}{\Delta t} + \frac{F_{j+\frac{1}{2}}(U^{n+\frac{1}{2}}) - F_{j-\frac{1}{2}}(U^{n+\frac{1}{2}})}{\Delta x} + Q_j U^{n+1} = 0, \tag{24}$$

where $F_{j\pm 1/2}(U^{n+\frac{1}{2}})$ is the numerical flux

$$F_{j+\frac{1}{2}}(U^{n+\frac{1}{2}}) = \frac{1}{2}\left(F_{j+\frac{1}{2}}^+(U^{n+\frac{1}{2}}) + F_{j+\frac{1}{2}}^-(U^{n+\frac{1}{2}})\right) \tag{25}$$

and

$$F_{j+\frac{1}{2}}^+(U^{n+\frac{1}{2}}) = \begin{pmatrix} (\rho_\varepsilon \mathbf{u}_\varepsilon)_j^{n+1} + A_{j+\frac{1}{2}}^n \rho_{\varepsilon j}^n \\ (\rho_\varepsilon \mathbf{u}_\varepsilon \otimes \mathbf{u}_\varepsilon)_j^n + \alpha p(\rho_{\varepsilon j}^n) + A_{j+\frac{1}{2}}^n (\rho_\varepsilon \mathbf{u}_\varepsilon)_j^n \end{pmatrix},$$

8

$$F_{j+\frac{1}{2}}^{-}(U^{n+\frac{1}{2}}) = \begin{pmatrix} (\rho_\varepsilon \mathbf{u}_\varepsilon)_{j+1}^{n+1} - A_{j+\frac{1}{2}}^{n} \rho_{\varepsilon j+1}^{n} \\ (\rho_\varepsilon \mathbf{u}_\varepsilon \otimes \mathbf{u}_\varepsilon)_{j+1}^{n} + \alpha p(\rho_{\varepsilon j+1}^{n}) - A_{j+\frac{1}{2}}^{n} (\rho_\varepsilon \mathbf{u}_\varepsilon)_{j+1}^{n} \end{pmatrix}$$

and

$$QU_j^{n+1} = \begin{pmatrix} 0 \\ \frac{1-\alpha\varepsilon^2}{\varepsilon^2} \frac{1}{2\Delta x} \left(P(\rho_{\varepsilon j+1}^{n+1}) - P(\rho_{\varepsilon j-1}^{n+1}) \right) \end{pmatrix}.$$

Let

$$\mathbf{q} = \rho\mathbf{u}, \tag{26}$$

and $F^{(1)}, F^{(2)}$ denote the first and second element of F respectively, we can rewrite the momentum discretization in (24) as follows:

$$\mathbf{q}_{\varepsilon j}^{n+1} = \mathbf{q}_{\varepsilon j}^{n} - \Delta t D_j^x F^{(2)}(\rho_\varepsilon^n, \mathbf{u}_\varepsilon^n) - \frac{1-\alpha\varepsilon^2}{\varepsilon^2} \frac{\Delta t}{2\Delta x} \left(p(\rho_{\varepsilon j+1}^{n+1}) - p(\rho_{\varepsilon j-1}^{n+1}) \right). \tag{27}$$

Here

$$D_j^x u = \frac{u_{j+1/2} - u_{j-1/2}}{\Delta x}.$$

By substituting (27) into the density equation in (24), one gets

$$\rho_{\varepsilon j}^{n+1} - \frac{(1-\alpha\varepsilon^2)\Delta t^2}{4\varepsilon^2 \Delta x^2} \left(p(\rho_{\varepsilon j+2}^{n+1}) - 2p(\rho_{\varepsilon j}^{n+1}) + p(\rho_{\varepsilon j-2}^{n+1}) \right) = D\phi(\rho_\varepsilon^n, \mathbf{q}_\varepsilon^n), \tag{28}$$

where

$$D\phi(\rho_\varepsilon^n, \mathbf{q}_\varepsilon^n) = \rho_\varepsilon^n - \Delta t D_j^x F^{(1)}(\rho_\varepsilon^n, \mathbf{u}_\varepsilon^n) + \frac{\Delta t^2}{2\Delta x} \left(D_{j+1}^x - D_{j-1}^x \right) F^{(2)}(\rho_\varepsilon^n, \mathbf{u}_\varepsilon^n) \tag{29}$$

is a discretization of $\phi(\rho_\varepsilon^n, \mathbf{u}_\varepsilon^n)$ in (10). We notice that (28) is a discretization of the elliptic equation (11). We can update $\mathbf{q}_\varepsilon^{n+1}$ through (27) afterwards.

To obtain ρ_ε^{n+1} in (28), a nonlinear system of equations needs to be solved. One possible way to simplify it is to replace $\nabla P(\rho_\varepsilon^{n+1})$ by $P'(\rho_\varepsilon^n)\nabla\rho_\varepsilon^{n+1}$, so that the following linear system is obtained:

$$\rho_{\varepsilon j}^{n+1} - \frac{(1-\alpha\varepsilon^2)\Delta t^2}{4\varepsilon^2 \Delta x^2} \left(p'(\rho_{\varepsilon j+1}^n)\left(\rho_{\varepsilon j+2}^{n+1} - \rho_{\varepsilon j}^{n+1}\right) - p'(\rho_{\varepsilon j-1}^n)\left(\rho_{\varepsilon j}^{n+1} - \rho_{\varepsilon j-2}^{n+1}\right) \right)$$
$$= D\phi(\rho_\varepsilon^n, \mathbf{q}_\varepsilon^n). \tag{30}$$

This is a five point scheme which is too much diffusive, especially near the shock. One possible improvement is that instead of (30), we use the following three

9

points discretization

$$\rho_{\varepsilon j}^{n+1} - \frac{(1-\alpha\varepsilon^2)\Delta t^2}{\varepsilon^2 \Delta x^2}\left(p'(\rho_{\varepsilon j+1}^n)(\rho_{\varepsilon j+1}^{n+1}-\rho_{\varepsilon j}^{n+1}) - p'(\rho_{\varepsilon j}^n)(\rho_{\varepsilon j}^{n+1}-\rho_{\varepsilon j-1}^{n+1})\right)$$
$$= D\phi(\rho_\varepsilon^n, \mathbf{q}_\varepsilon^n). \quad (31)$$

After obtaining ρ_ε^{n+1}, we can substitute it into (27) to get $\mathbf{q}_{\varepsilon j}^{n+1}$.

To summarize, three schemes are proposed here: (28), (27); (30), (27) and (31), (27). To investigate the AP property, we take (30), (27) as an example. The proofs for the other two schemes are similar. By substituting the following expansion

$$\rho_{\varepsilon j}^n = \rho_{0c}^n + \varepsilon^2 \rho_{(2)j}^n + \cdots, \qquad \mathbf{q}_{\varepsilon j}^n = \mathbf{q}_{0c}^n + \varepsilon \mathbf{q}_{(2)j}^n + \cdots, \qquad (32)$$

into (30), the $O(\frac{1}{\varepsilon^2})$ terms give that $\rho_{(0)j}^{n+1} = \rho_{0c}^{n+1}$ is constant in space by using the periodic boundary condition, and thus:

$$\rho_{\varepsilon j}^{n+1} = \rho_{(0)c}^{n+1} + \varepsilon^2 \rho_{(2)j}^{n+1} + \cdots.$$

Summing (30) over all the grid points, one gets

$$\rho_{0c}^{n+1} = \rho_{0c}^n = \rho_{0c}, \qquad (33a)$$

which implies that ρ_0 is independent of time and space. Thus, the $O(1)$ terms of (30) are

$$p'(\rho_{0c}^n)(\rho_{(2)j+2}^{n+1}-\rho_{(2)j}^{n+1}) - p'(\rho_{0c}^n)(\rho_{(2)j}^{n+1}-\rho_{(2)j-1}^{n+1}) = 0,$$

by recalling that the $O(1)$ terms of both ρ_ε^n and $\mathbf{q}_\varepsilon^n$ are constant in space. Then the periodic boundary condition gives

$$\rho_{(2)j}^{n+1} = \rho_{(2)c}^{n+1}, \qquad (33b)$$

which gives that $\rho_{(2)}^{n+1}$ is also independent of space. Therefore from (2), (27),

$$\mathbf{q}_{0j}^{n+1} = \mathbf{q}_{0j}^n = \mathbf{q}_{0c}^n. \qquad (33c)$$

In one dimension, (33) is the discretization of (15), (16), (18) when periodic boundary conditions apply and thus is consistent with the incompressible limit. In fact all the three methods proposed here are AP.

4 Full time and space discretization: Two dimensional case

We consider the domain $\Omega = [0,1] \times [0,1]$. For M_1, M_2 two positive integers, we use a uniform spatial mesh $\Delta x = 1/M_1, \Delta y = 1/M_2$. The grid points are

$$(x_i, y_j) := (i\Delta x, j\Delta y), \qquad i = 0, \cdots, M_1; j = 0, \cdots, M_2$$

Now $U = (\rho_\varepsilon, \mathbf{q}_\varepsilon^{(1)}, \mathbf{q}_\varepsilon^{(2)})^T$ and $U_{i,j}$ is the numerical approximation of $U(x_i, y_j)$. Let

$$G_1(U) = \begin{pmatrix} \rho_\varepsilon \mathbf{u}_{\varepsilon 1} \\ \rho_\varepsilon \mathbf{u}_1^2 + \alpha p(\rho_\varepsilon) \\ \rho_\varepsilon \mathbf{u}_1 \mathbf{u}_2 \end{pmatrix}, \quad G_2(U) = \begin{pmatrix} \rho_\varepsilon \mathbf{u}_{\varepsilon 2} \\ \rho_\varepsilon \mathbf{u}_1 \mathbf{u}_2 \\ \rho_\varepsilon \mathbf{u}_2^2 + \alpha p(\rho_\varepsilon) \end{pmatrix}. \qquad (34)$$

and

$$Q = \frac{1 - \alpha \varepsilon^2}{\varepsilon^2} \begin{pmatrix} 0 & 0 & 0 \\ \partial_x P & 0 & 0 \\ \partial_y P & 0 & 0 \end{pmatrix}.$$

Eq. (19) can be written as

$$\partial_t U + \partial_x G_1(U) + \partial_y G_2(U) + QU = 0.$$

Denote

$$G_1(U^{n+\frac{1}{2}}) = \begin{pmatrix} (\rho_\varepsilon \mathbf{u}_{\varepsilon 1})^{n+1} \\ \rho_\varepsilon^n (\mathbf{u}_{\varepsilon 1}^n)^2 + \alpha p(\rho_\varepsilon^n) \\ \rho_\varepsilon^n \mathbf{u}_{\varepsilon 1}^n \mathbf{u}_2^n \end{pmatrix}, \qquad G_2(U^{n+\frac{1}{2}}) = \begin{pmatrix} (\rho_\varepsilon \mathbf{u}_{\varepsilon 2})^{n+1} \\ \rho_\varepsilon^n \mathbf{u}_{\varepsilon 1}^n \mathbf{u}_{\varepsilon 2}^n \\ \rho_\varepsilon^n (\mathbf{u}_{\varepsilon 2}^n)^2 + \alpha p(\rho_\varepsilon^n) \end{pmatrix},$$

$$\tilde{Q} = \begin{pmatrix} 0 & 0 & 0 \\ \frac{1-\alpha\varepsilon^2}{\varepsilon^2} D^x \hat{P} & 0 & 0 \\ \frac{1-\alpha\varepsilon^2}{\varepsilon^2} D^y \hat{P} & 0 & 0 \end{pmatrix},$$

$$D_{ij}^x u = \frac{u_{ij+1} - u_{ij-1}}{2\Delta x}, \qquad D_{ij}^y u = \frac{u_{i+1j} - u_{i-1j}}{2\Delta y}.$$

Now the eigenvalues of the two one-dimensional hyperbolic equations are

$$\lambda^{(1)} = \mathbf{u}_1, \mathbf{u}_1 \pm \sqrt{\alpha p'(\rho_\varepsilon)}, \qquad \lambda^{(2)} = \mathbf{u}_2, \mathbf{u}_2 \pm \sqrt{\alpha p'(\rho_\varepsilon)}.$$

The fully discrete scheme for the two dimensional problem is

$$\frac{U_{ij}^{n+1} - U_{ij}^n}{\Delta t} + D_{ij}^x G_1(U^{n+1/2}) + \frac{1}{2}\left(A_{i-\frac{1}{2},j}D_{ij-}^x - A_{i+\frac{1}{2},j}D_{ij+}^x\right)U^n$$

$$+D_{ij}^y G_2(U^{n+1/2}) + \frac{1}{2}\left(A_{i,j-\frac{1}{2}}D_{ij-}^y - A_{i,j+\frac{1}{2}}D_{ij+}^y\right)U^n + \tilde{Q}U_{ij}^{n+1} = 0, \qquad (35)$$

where

$$D_{ij-}^x u = \frac{u_{ij} - u_{i-1j}}{\Delta x}, \quad (D_{ij+}^x u) = \frac{u_{i+1j} - u_{ij}}{\Delta x},$$

$$D_{ij-}^y u = \frac{u_{ij} - u_{ij-1}}{\Delta y}, \quad D_{ij+}^y u = \frac{u_{ij+1} - u_{ij}}{\Delta y},$$

and

$$A_{i+\frac{1}{2},j}^n = \max\{|\lambda_{ij}^{(1)}|, |\lambda_{i+1,j}^{(1)}|, |\lambda_{ij}^{(2)}|, |\lambda_{i+1,j}^{(2)}|\},$$

$$A_{i,j+\frac{1}{2}}^n = \max\{|\lambda_{ij}^{(1)}|, |\lambda_{i,j+1}^{(1)}|, |\lambda_{ij}^{(2)}|, |\lambda_{i,j+1}^{(2)}|\}. \qquad (36)$$

Let $\mathbf{q}_\varepsilon$ be like in (27). Like in one dimension, we can substitute the expressions of $\mathbf{q}_{1ij}^{n+1}, \mathbf{q}_{2ij}^{n+1}$ into the density equation and get the following discretized elliptic equation,

$$\rho_{\varepsilon ij}^{n+1} - \frac{(1-\alpha\varepsilon^2)\Delta t^2}{4\varepsilon^2}\left(\frac{1}{\Delta x^2}\left(P(\rho_{\varepsilon i+2,j}^{n+1}) - 2P(\rho_{\varepsilon i,j}^{n+1}) + P(\rho_{\varepsilon i-2,j}^{n+1})\right) + \qquad (37)\right.$$

$$\left.\frac{1}{\Delta y^2}\left(P(\rho_{\varepsilon i,j+2}^{n+1}) - 2P(\rho_{\varepsilon i,j}^{n+1}) + P(\rho_{\varepsilon i,j-2}^{n+1})\right)\right) = D\phi_{ij}(\rho_\varepsilon^n, \mathbf{q}_{1\varepsilon}^n, \mathbf{q}_{2\varepsilon}^n),$$

where

$$D\phi_{ij}(\rho_\varepsilon^n, \mathbf{q}_{1\varepsilon}^n, \mathbf{q}_{2\varepsilon}^n)$$

$$= \rho_\varepsilon^n - \Delta t\left(D_{ij}^x \mathbf{q}_{\varepsilon 1}^n + D_{ij}^y \mathbf{q}_{\varepsilon 2}^n\right.$$

$$+\frac{1}{2}\left(A_{i-\frac{1}{2}}D_{ij-}^x - A_{i+\frac{1}{2},j}D_{ij+}^x + A_{i,j-\frac{1}{2}}D_{ij-}^y - A_{i,j+\frac{1}{2}}D_{ij+}^y\right)\rho_\varepsilon^n\right)$$

$$+\Delta t^2\left(D_{ij}^x D_{ij}^x\left(\rho_\varepsilon^n(\mathbf{u}_{\varepsilon 1}^n)^2 + \alpha p(\rho_\varepsilon^n)\right) + D_{ij}^y D_{ij}^y\left(\rho_\varepsilon^n(\mathbf{u}_{\varepsilon 2}^n)^2 + \alpha p(\rho_\varepsilon^n)\right)\right.$$

$$+(D_{ij}^x D_{ij}^y + D_{ij}^y D_{ij}^x)\rho_\varepsilon^n \mathbf{u}_{\varepsilon 1}^n \mathbf{u}_{\varepsilon 2}^n + \frac{1}{2}D_{ij}^x(A_{i-\frac{1}{2},j}D_{ij-}^x - A_{i+\frac{1}{2},j}D_{ij+}^x)\mathbf{q}_{\varepsilon 1}^n$$

$$+\frac{1}{2}D_{ij}^y(A_{i-\frac{1}{2},j}D_{ij-}^x - A_{i+\frac{1}{2},j}D_{ij+}^x)\mathbf{q}_{\varepsilon 2}^n + \frac{1}{2}D_{ij}^x(A_{i,j-\frac{1}{2}}D_{ij-}^y - A_{i,j+\frac{1}{2}}D_{ij+}^y)\mathbf{q}_{\varepsilon 1}^n$$

$$+\frac{1}{2}D_{ij}^y(A_{i,j-\frac{1}{2}}D_{ij-}^y - A_{i,j+\frac{1}{2}}D_{ij+}^y)\mathbf{q}_{\varepsilon 2}^n\right).$$

$$(38)$$

12

After obtaining ρ_{ij}^{n+1} by (37), $\mathbf{q}_{1ij}^{n+1}, \mathbf{q}_{2ij}^{n+1}$ can be updated by the momentum equation afterwards.

Similar to the one-dimensional case, the modified diffusion operator using a reduced stencil is as follows:

$$\rho_{\varepsilon ij}^{n+1} - \Delta t^2 \frac{1 - \alpha\varepsilon^2}{\varepsilon^2} \times$$

$$\times \left(\frac{1}{\Delta x^2} \left(P'(\rho_{\varepsilon i,j+1}^n)\left(\rho_{\varepsilon i,j+1}^{n+1} - \rho_{\varepsilon i,j}^{n+1}\right) - P'(\rho_{\varepsilon i,j}^n)\left(\rho_{\varepsilon i,j}^{n+1} - \rho_{\varepsilon i,j-1}^{n+1}\right)\right) \right.$$

$$\left. + \frac{1}{\Delta y^2}\left(P'(\rho_{\varepsilon i+1,j}^n)\left(\rho_{\varepsilon i+1,j}^{n+1} - \rho_{\varepsilon i,j}^{n+1}\right) - P'(\rho_{\varepsilon i,j}^n)\left(\rho_{\varepsilon i,j}^{n+1} - \rho_{\varepsilon i-1,j}^{n+1}\right)\right)\right)$$

$$= \phi(\rho_\varepsilon^n, \mathbf{q}_{1\varepsilon}^n, \mathbf{q}_{2\varepsilon}^n). \tag{39}$$

Now we prove the AP property of our fully discrete scheme. Here only well-prepared initial conditions are considered, which means that there will be no shock forming in the solution. Then α can be chosen to be 0 to minimize the introduced numerical viscosity. Assuming that the expansions of $\rho_\varepsilon, \mathbf{u}_\varepsilon$ in (12) hold at time t^n, when $\varepsilon \to 0$, the $O(\frac{1}{\varepsilon^2})$ terms of (39) give

$$\frac{1}{\Delta x^2}\left(P'(\rho_{0i,j+1}^n)\left(\rho_{0i,j+1}^{n+1} - \rho_{0i,j}^{n+1}\right) - P'(\rho_{0i,j}^n)\left(\rho_{0i,j}^{n+1} - \rho_{0i,j-1}^{n+1}\right)\right)$$

$$+ \frac{1}{\Delta y^2}\left(P'(\rho_{0i+1,j}^n)\left(\rho_{0i+1,j}^{n+1} - \rho_{0i,j}^{n+1}\right) - P'(\rho_{0i,j}^n)\left(\rho_{0i,j}^{n+1} - \rho_{0i-1,j}^{n+1}\right)\right) = 0.$$

When using periodic boundary conditions, one gets $\rho_{0ij}^{n+1} = \rho_{0c}^{n+1}$ from (2). The time independence of ρ_0^{n+1}, similar to the one dimensional case, can be obtained by summing (39) over all the grid points. Accordingly we have

$$\rho_{\varepsilon ij}^{n+1} = \rho_{0c}^n + \varepsilon^2 \rho_{(2)ij}^{n+1} + \cdots. \tag{40}$$

To prove the limiting behavior of $\mathbf{u}_{\varepsilon 1}, \mathbf{u}_{\varepsilon 2}$, we do not want to use the density equation because the diffusion operator with reduced stencil does not allow us to find the corresponding density equation. Therefore, we consider the $O(1)$ term of (39),

$$\rho_{0ij}^{n+1} - \Delta t^2 \times$$

$$\times \left(\frac{1}{\Delta x^2}\left(P'(\rho_{0c}^n)\left(\rho_{(2)i,j+1}^{n+1} - \rho_{(2)i,j}^{n+1}\right) - P'(\rho_{0c}^n)\left(\rho_{(2)i,j}^{n+1} - \rho_{(2)i,j-1}^{n+1}\right)\right)\right.$$

$$\left. + \frac{1}{\Delta y^2}\left(P'(\rho_{0c}^n)\left(\rho_{(2)i+1,j}^{n+1} - \rho_{(2)i,j}^{n+1}\right) - P'(\rho_{0c}^n)\left(\rho_{(2)i,j}^{n+1} - \rho_{(2)i-1,j}^{n+1}\right)\right)\right)$$

$$= \phi(\rho_0^n, \mathbf{q}_{10}^n, \mathbf{q}_{20}^n). \tag{41}$$

13

Moreover, noting the fact that

$$
\begin{aligned}
D_{ij}^x P(\rho_\varepsilon^{n+1}) &= D_{ij}^x P(\rho_{0c}^n + \varepsilon^2 \rho_{(2)}^{n+1} + o(\varepsilon^2)) \\
&= D_{ij}^x P(\rho_{0c}^n) + \varepsilon^2 D_{ij}^x \left(\rho_{(2)}^{n+1} P'(\rho_{0c}^n) \right) + o(\varepsilon^2), \\
&= \varepsilon^2 D_{ij}^x \left(\rho_{(2)}^{n+1} P'(\rho_{0c}^n) \right) + o(\varepsilon^2),
\end{aligned}
$$

and similarly,
$$
D_{ij}^y P(\rho_\varepsilon^{n+1}) = \varepsilon^2 D_{ij}^y \left(\rho_{(2)}^{n+1} P'(\rho_{0c}^n) \right) + o(\varepsilon^2),
$$

the $O(1)$ terms of the momentum equations of (35) become

$$
\frac{\mathbf{q}_{01ij}^{n+1} - \mathbf{q}_{01ij}^n}{\Delta t} + D_{ij}^x \left(\frac{\mathbf{q}_{01}^2}{\rho_0} \right)^n + D_{ij}^y \left(\frac{\mathbf{q}_{01}\mathbf{q}_{02}}{\rho_0} \right)^n + \frac{1}{2}\left(A_{i-\frac{1}{2},j} D_{ij-}^x - A_{i+\frac{1}{2},j} D_{ij+}^x \right.
$$
$$
\left. + A_{i,j-\frac{1}{2}} D_{ij-}^y - A_{i,j+\frac{1}{2}} D_{ij+}^y \right) \mathbf{q}_{01} = D_{ij}^x \left(P'(\rho_{0c}^{n+1}) \rho_{(2)}^{n+1} \right), \quad (42a)
$$

$$
\frac{\mathbf{q}_{02ij}^{n+1} - \mathbf{q}_{02ij}^n}{\Delta t} + D_{ij}^x \left(\frac{\mathbf{q}_{01}\mathbf{q}_{02}}{\rho_0} \right)^n + D_{ij}^y \left(\frac{\mathbf{q}_{02}^2}{\rho_0} \right)^n + \frac{1}{2}\left(A_{i-\frac{1}{2},j} D_{ij-}^x - A_{i+\frac{1}{2},j} D_{ij+}^x \right.
$$
$$
\left. + A_{i,j-\frac{1}{2}} D_{ij-}^y - A_{i,j+\frac{1}{2}} D_{ij+}^y \right) \mathbf{q}_{02} = D_{ij}^y \left(P'(\rho_{0c}^{n+1}) \rho_{(2)}^{n+1} \right). \quad (42b)
$$

Comparing (41) with $\Delta t * \left(D_{ij}^x (42a) + D_{ij}^y (42b) \right)$, one gets

$$
D_{ij}^x \mathbf{q}_{01}^{n+1} + D_{ij}^y \mathbf{q}_{02}^{n+1} = O(\Delta x \Delta t), \tag{43}
$$

which is an approximation of (16). Moreover, it is obvious that (42) is a discretization of (18). Thus we obtain a full discretization of (4) in the limit $\varepsilon \to 0$. Therefore, the two-dimensional scheme is also AP.

5   The ad-hoc parameter

In this section we illustrate how to choose Δt and the parameter α by considering the simple state equation $P(\rho_\varepsilon) = \rho_\varepsilon$. In this context, the fully discrete scheme (24) can be written as

$$
\begin{cases}
\frac{\rho_\varepsilon^{n+1} - \rho_\varepsilon^n}{\Delta t} + \nabla \cdot \mathbf{q}_\varepsilon^{n+1} - \nabla \cdot \mathbf{q}_\varepsilon^n + \tilde{\nabla} \cdot \mathbf{q}_\varepsilon^n = 0, \\
\frac{\mathbf{q}_\varepsilon^{n+1} - \mathbf{q}_\varepsilon^n}{\Delta t} + \tilde{\nabla}\left(\rho_\varepsilon^n \mathbf{u}_\varepsilon^n \otimes \mathbf{u}_\varepsilon^n + \alpha \rho_\varepsilon^n \right) + \frac{1-\alpha\varepsilon^2}{\varepsilon^2} \nabla \rho_\varepsilon^{n+1} = 0.
\end{cases} \tag{44}
$$

14

where ∇ is the centered difference while $\tilde{\nabla}$ stands for the difference of fluxes. The latter is defined as follows (in one space-dimension for simplicity):

$$(\tilde{\nabla} \cdot F(U^n))_j = \frac{F_{j+\frac{1}{2}}(U^n) - F_{j-\frac{1}{2}}(U^n)}{\Delta x},$$

where the flux $F_{j\pm1/2}$ is defined as in (25). By substituting $\nabla \cdot (\mathbf{q}_\varepsilon^{n+1} - \mathbf{q}^n)$ from the momentum equation of (44) into its density equation, one gets

$$\frac{\rho_\varepsilon^{n+1} - \rho_\varepsilon^n}{\Delta t} + \tilde{\nabla} \cdot \mathbf{q}_\varepsilon^n - \Delta t \frac{1 - \alpha\varepsilon^2}{\varepsilon^2} \Delta\rho_\varepsilon^{n+1} - \Delta t \nabla \cdot \tilde{\nabla}(\rho_\varepsilon^n \mathbf{u}_\varepsilon^n \otimes \mathbf{u}_\varepsilon^n + \alpha\rho_\varepsilon^n) = 0. \quad (45)$$

The $O(\Delta t)$ terms behave like a diffusion term which suppresses the oscillations at the discontinuity. Assuming that we use a first order explicit LLF scheme, the diffusions needed to damp out the oscillations in the mass and momentum equations are respectively:

$$\frac{1}{2}(|\mathbf{u}_\varepsilon^n| + \frac{1}{\varepsilon})\Delta x \Delta\rho_\varepsilon^n, \qquad \frac{1}{2}(|\mathbf{u}_\varepsilon^n| + \frac{1}{\varepsilon})\Delta x \Delta\mathbf{q}_\varepsilon^n. \quad (46)$$

Here in (45), besides the $O(\Delta t)$ terms, $\tilde{\nabla} \cdot \mathbf{q}_\varepsilon^n$ also includes some numerical dissipation. By noting

$$\rho_\varepsilon^{n+1} = \rho_\varepsilon^n - \Delta t \nabla \cdot \mathbf{q}_\varepsilon^{n+1} + O(\Delta t \Delta x),$$

the diffusion for ρ_ε now is

$$\left(\frac{1}{2}(|\mathbf{u}_\varepsilon| + \sqrt{\alpha})\Delta x + \frac{\Delta t}{\varepsilon^2}\right)\Delta\rho_\varepsilon^n + \Delta t \Delta(\rho_\varepsilon^n \mathbf{u}_\varepsilon^n \otimes \mathbf{u}_\varepsilon^n) \quad (47)$$

plus some higher order terms. Moreover, the diffusion for $\mathbf{q}_\varepsilon$ is

$$\frac{1}{2}(|\mathbf{u}_\varepsilon| + \sqrt{\alpha})\Delta x \Delta\mathbf{q}_\varepsilon^n + \Delta t \frac{1 - \alpha\varepsilon^2}{\varepsilon^2}\Delta\mathbf{q}_\varepsilon^n \quad (48)$$

and some higher order terms. Comparing (46) and (47), (48), in order to suppress the oscillations at discontinuities we only need to have

$$\frac{1}{2}(|\mathbf{u}_\varepsilon^n| + \sqrt{\alpha})\Delta x + \frac{1 - \alpha\varepsilon^2}{\varepsilon^2}\Delta t \geq \frac{1}{2}(|\mathbf{u}_\varepsilon^n| + \frac{1}{\varepsilon})\Delta x,$$

that is

$$\Delta t \geq \frac{\frac{1}{2}\varepsilon\Delta x}{1 + \sqrt{\alpha}\varepsilon}. \quad (49)$$

15

Moreover the CFL condition for the explicit part is

$$\Delta t \leq \sigma \frac{\Delta x}{\max\{|\mathbf{u}_\varepsilon| + \sqrt{\alpha}\}}, \tag{50}$$

where σ is the Courant number which is less than 1. We usually choose σ to be 0.5. Then the parameter α should satisfy

$$\frac{\Delta x}{2\Delta t} - \frac{1}{\varepsilon} \leq \sqrt{\alpha} \leq \frac{\sigma \Delta x}{\Delta t} - \max\{|\mathbf{u}^n|_\varepsilon\} \tag{51}$$

according to (49), (50). Then the following constraint on Δt should hold if we want the scheme to be stable and non-oscillatory

$$\max\{|\mathbf{u}_\varepsilon^n|\} + \frac{\Delta x}{2\Delta t} \leq \frac{\sigma \Delta x}{\Delta t} + \frac{1}{\varepsilon}. \tag{52}$$

The reason for the occurence of nonphysical oscillations when $\alpha = 0$ lies in the fact that the diffusion is not large enough. In this case, with a simple reduction of Δt, it is likely that the diffusion can no longer suppress the oscillations. This is why we need to introduce α to control the oscillations. But, from the analysis, no matter the value of α, as long as it is less than $1/\varepsilon^2$, the diffusion can never be sufficient when $\Delta t \leq \frac{1}{4}\varepsilon\Delta x$. In summary there is no specific way of choosing $\alpha < 1/\varepsilon$ that can guarantee that the nonphysical oscillations will disappear in any case. For well-prepared initial conditions in the low Mach number regime, because there is no shock formation in the solution, it is better to choose α as small as possible to get better accuracy, but if strong shocks exist in the solution, α should be big enough to suppress the oscillations. This is why the choice of α depends on the considered problem.

6 Numerical results

Three numerical examples will allow us to test the performances of the proposed schemes. In fact, three schemes are proposed in section 3 and 4, for example in one dimension: the scheme (24) without linearizing $\nabla P(\rho_\varepsilon^{n+1})$ is denoted by "NL". We need to use Newton iterations to solve the nonlinear system. When $\nabla P(\rho_\varepsilon^{n+1})$ is approximated by $P'(\rho_\varepsilon^n)\nabla P(\rho_\varepsilon^{n+1})$, the unknowns become a linear system. This scheme is represented by "L". "LD" denotes the scheme with the narrower stencil (31). Here we use well-prepared initial conditions of the form (3) and $\alpha = 1$ for all the test cases.

In one dimension, let the computational domain be $[a,b]$ and the mesh size be Δx. The grid points are

$$x_j = a + (j-1)\Delta x.$$

In the following tables, the L^2 norm of the relative error between the reference solutions u and the numerical ones U

$$e(U) = \frac{\|U - u\|_{L^2}}{\|u\|_{L^2}} = \frac{\frac{1}{M}\left(\sum_j |U_j - u(x_j)|^2\right)^{\frac{1}{2}}}{\frac{1}{M_e}\left(\sum_i |u(x_i)|^2\right)^{\frac{1}{2}}}$$

are displayed.

Example 1 $P(\rho_\varepsilon)$ and the initial conditions are chosen as

$$P(\rho_\varepsilon) = \rho_\varepsilon^2,$$

$$
\begin{array}{lll}
\rho_\varepsilon(x,0) = 1, & p_\varepsilon(x,0) = 1 - \varepsilon^2/2 & x \in [0,0.2] \cup [0.8,1]; \\
\rho_\varepsilon(x,0) = 1 + \varepsilon^2, & p_\varepsilon(x,0) = 1 & x \in (0.2,0.3]; \\
\rho_\varepsilon(x,0) = 1, & p_\varepsilon(x,0) = 1 + \varepsilon^2/2 & x \in (0.3,0.7] \\
\rho_\varepsilon(x,0) = 1 - \varepsilon^2, & p_\varepsilon(x,0) = 1 & x \in (0.7,0.8]
\end{array}
$$

This example consists of several Riemann problems. Shocks and contact discontinuities are stronger when ε is bigger. We first check the difference of the three schemes (28), (30) and (31). The CFL condition for the linearized reduced stencil scheme (31) is discussed in (ii) and a fixed Courant number independent of ε is found numerically. Compared with the first order ICE method using local Lax-Friedrich discretization for (5), the improvement of removing nonphysical oscillation of our scheme is shown. We investigate the effect of α for different values of ε in (iii). In (iv), when $\alpha = 1$, we numerically test the uniform convergence order. Finally, the AP property and its advantages are demonstrated in (v) by comparing with the fully explicit Lax-Fridrich scheme for the initial Isentropic Euler equation (1).

When $\varepsilon = 0.1$, the initial density and momentum are displayed in Figure 1 and we can see the discontinuities clearly.

(i) In this example, we choose $\varepsilon = 0.8, 0.3, 0.05$ corresponding to the compressible, intermediate and incompressible regimes. The numerical results at $T = 0.05$ of "NL", "L" and "LD" are represented in Figure 2. Here Δt is chosen to make all these three schemes stable and diminishing Δt only will not improve much the numerical accuracy. The reference solution is calculated by an explicit Lax-Friedrich method [19, 20] with $\Delta x = 1/500, \Delta t =$
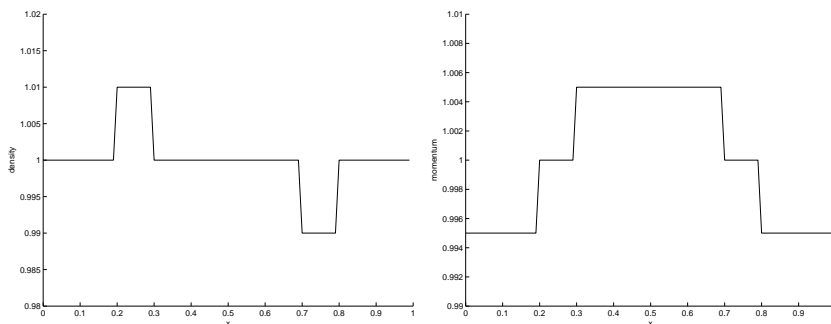
Figure 1: Example 1. When $\varepsilon = 0.1$, the initial density and momentum are displayed.

1/20000. We can see that all these three methods can capture the right shock speed. The results of the three schemes are quite close, which implies that the linearization idea does simplify the scheme but the "LD" scheme does not really introduce less diffusion. When ε is small, though we can no longer capture all the details of the waves, the error is of the order Δx which is the maximum information one can expect. Numerically, for different scales of ε, there is not much difference between these three methods. Thus in the following one dimensional examples, we only test the performance of the "LD" scheme.

(ii) Because of the explicit treatment of the flux terms in the momentum equation, the stability of the 'LD' scheme can be only guaranteed under the following CFL condition

$$\Delta t \leq \sigma \min_{i} \frac{\Delta x}{|\mathbf{u}_i| + \sqrt{\alpha P'(\rho_\varepsilon)}}. \tag{53}$$

Here $0 < \sigma < 1$ is the Courant number and is set up at initialization. Consistently with the fact that these three methods are AP, the Courant number does not depend on ε. Indeed, below, we numerically verify that σ is independent of ε. For $\varepsilon = 0.8, 0.3, 0.05$, the numerical Courant numbers are displayed in Table 1 and we can see numerically that the biggest allowed $\max\{u\}\frac{\Delta t}{\Delta x}$ are close to 1 for all ε's. Therefore, $\sigma = 0.9$ is enough to guarantee stability and is numerically shown to be independent of ε. By contrast, the explicit local Lax-Friedrich scheme for the original Euler equation has a stability condition which becomes more and more restrictive as
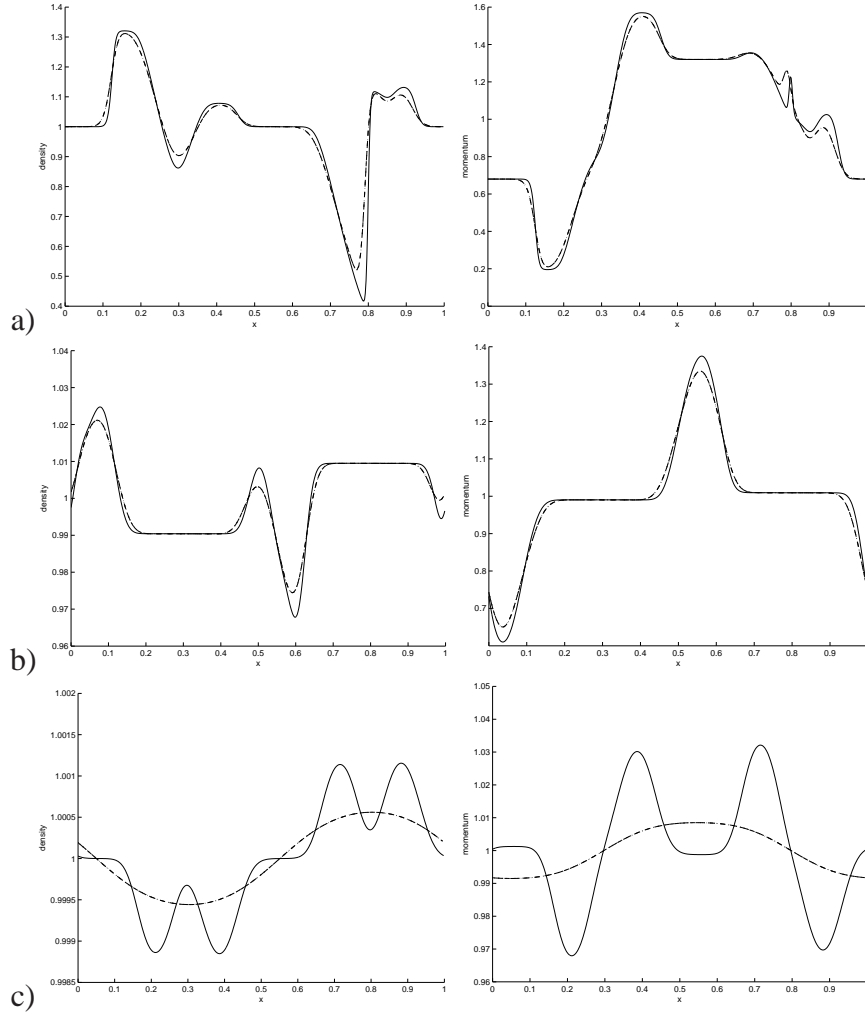
18

Figure 2: Example 1. When $T = 0.05, \Delta x = 1/200, \Delta t = 1/2000$, the density and momentum of the "NL", "L" and "LD" schemes for isentropic Euler equation are represented respectively by dashed, dash dotted, and dotted lines. The solid line is the reference solution calculated by an explicit Lax-Friedrich method [19, 20] with $\Delta x = 1/500, \Delta t = 1/20000$. a): $\varepsilon = 0.8$; b): $\varepsilon = 0.3$; c): $\varepsilon = 0.05$. Left: density; Right: momentum. For all ε's, these three lines are so close to each other that '-.-.' and '...' are not visible in the figure.

19

ε goes to zero. Thus the CFL condition of the standard hyperbolic solver $\Delta t = O(\varepsilon \Delta x)$ is considerably improved.

ε	$\max \lambda$	Δx	stableΔt	$\frac{\Delta x}{\Delta t}$	$u\frac{\Delta t}{\Delta x}$
0.8	4.24	1/100	1/340	3.40	1.25
0.8	6.35	1/200	1/970	4.85	1.31
0.8	6.58	1/400	1/2420	6.05	1.09
0.8	6.70	1/800	1/5460	6.82	0.982
0.3	2.64	1/100	1/260	2.60	1.02
0.3	2.70	1/200	1/510	2.55	1.06
0.3	2.76	1/400	1/1000	2.50	1.10
0.3	2.81	1/800	1/2050	2.56	1.10
0.05	2.43	1/100	1/260	2.60	0.93
0.05	2.44	1/200	1/490	2.45	1.00
0.05	2.45	1/400	1/960	2.40	1.02
0.05	2.46	1/800	1/1920	2.40	1.03

Table 1: Example 1. The numerical Courant numbers for different ε. Here $\max\{\lambda\}$ denotes the maximum of $\max\{\lambda_j\}$ defined in (22) until $T = 0.1$ for all time steps.

(iii) The classical ICE method even in its conservative form introduces some nonphysical oscillations, no matter how small the time step is. These oscillations cannot be diminished by decreasing the time step. Their amplitude becomes smaller as the mesh is refined as long as the scheme is stable. In this part we show that our method can suppress these oscillations numerically by choosing $\alpha = 1$. When $T = 0.01$, for $\varepsilon = 0.8, 0.3, 0.05$, the numerical results of both our method with $\alpha = 1$ and ICE calculated by $\Delta x = 1/200, \Delta t = 1/20000$ are displayed in Figure 3. The oscillations are more important for the ICE method and smooth away when $\alpha = 1$. We can see that numerical nonphysical oscillations occur in the results of the ICE method when $\varepsilon = 0.8, 0.3$, but disappear when ε becomes small. This can also be seen from (47), (48). When ε is small the diffusion introduced by the implicitness is bigger. These oscillations also go away as time goes on due to dissipation.

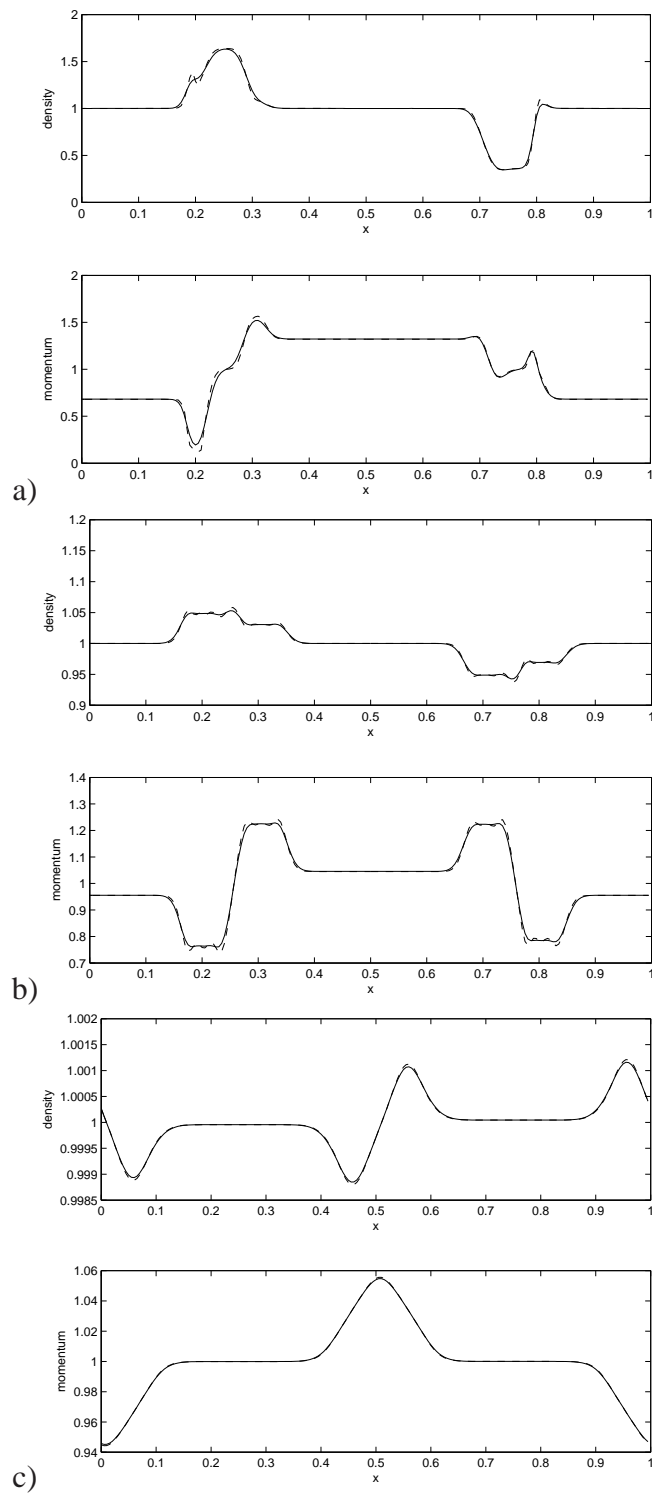(iv) When $\alpha = 1$, the relative errors of the "LD" scheme for different Δx, Δt

Figure 3: Example 1. When $T = 0.01$, the density and momentum for different ε are presented. The solid and dashed lines are the numerical results of our scheme and ICE with $\Delta x = 1/200, \Delta t = 1/20000$ respectively. a) $\varepsilon = 0.8$; b) $\varepsilon = 0.3$; c)$\varepsilon = 0.05$.

at time $T = 0.1$ are shown in Table 2. Here $\Delta x, \Delta t$ do not need to resolve ε and the reference solution is obtained by the explicit LLF scheme calculated with a very fine mesh $\Delta x = 1/1280, \Delta t = 1/128000$. We can see that good numerical approximations can be obtained without resolving the small ε. The convergence order is $1/2$ when $\Delta t/\Delta x$ is fixed, uniformly with respect to ε. This convergence order when there are discontinuities is the same as the explicit LLF [21]. We can see from Table 2 that refinement in the time step does not improve the accuracy much (provided the Courant number is appropriately small, like $\sigma = 0.7$). Take $\varepsilon = 0.8$ as an example. When $\Delta x = 1/320$, in order to obtain stability, Δt should be less than $1/1920$. It is demonstrated in Table 2 that the error calculated with $\Delta x = 1/320$ does not decrease much when Δt is changed from $1/2880$ to $1/12800$. Thus as long as the scheme is stable, we cannot use a smaller Δt to obtain a better accuracy. This feature is the same as for standard hyperbolic solvers.

ε	Δx	Δt	$e(\rho_\varepsilon)$	ratio	$e(p_\varepsilon)$	ratio
0.8	1/20	1/180	$9.739 * 10^{-1}$	-	1.197	-
0.8	1/40	1/360	$5.959 * 10^{-1}$	1.63	$7.484 * 10^{-1}$	1.16
0.8	1/80	1/720	$3.467 * 10^{-1}$	1.72	$4.180 * 10^{-1}$	1.31
0.8	1/160	1/1440	$1.985 * 10^{-1}$	1.75	$2.048 * 10^{-1}$	1.36
0.8	1/320	1/2880	$1.126 * 10^{-1}$	1.76	$8.477 * 10^{-2}$	1.79
0.8	1/320	1/12800	$1.126 * 10^{-1}$	-	$8.539 * 10^{-2}$	-
0.05	1/20	1/70	$4.679 * 10^{-3}$	-	$1.355 * 10^{-1}$	-
0.05	1/40	1/140	$3.305 * 10^{-3}$	1.42	$9.574 * 10^{-2}$	1.42
0.05	1/80	1/280	$2.353 * 10^{-3}$	1.40	$6.758 * 10^{-2}$	1.42
0.05	1/160	1/560	$1.655 * 10^{-3}$	1.42	$4.430 * 10^{-2}$	1.53
0.05	1/320	1/1120	$1.094 * 10^{-3}$	1.51	$2.538 * 10^{-2}$	1.75
0.05	1/320	1/12800	$6.012 * 10^{-4}$	-	$9.303 * 10^{-3}$	-

Table 2: Example 1. $T = 0.1$, the L^2 norm of the relative error between the reference solution which is calculated with a very fine mesh $\Delta x = 1/1280, \Delta t = 1/128000$ and the numerical results for different ε with different $\Delta x, \Delta t$ are displayed.

(v) We emphasize the AP property in this final part. For $\varepsilon = 0.005$, the numerical results at $T = 0.01$ with unresolved mesh $\Delta x = 1/20, \Delta t = 1/500$ and
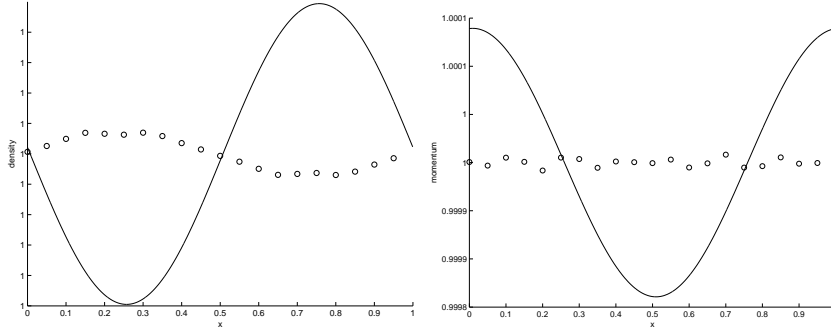
Figure 4: Example 1. By using the "LD" scheme, the density (left) and momentum (right) for $\varepsilon = 0.005$ at $T = 0.01$ are represented. The circles are the results for $\Delta x = 1/20, \Delta t = 1/500$ and the solid line is calculated with $\Delta x = 1/2000, \Delta t = 1/5000$.

resolved mesh $\Delta x = 1/2000, \Delta t = 1/5000$ are displayed in Figure 4, while the fully explicit Lax-Fridrich scheme is not stable with the same mesh size. We do capture the incompressible limit when $\Delta x, \Delta t$ do not resolve ε.

Example 2: In this example we simulate the evolution of two collision acoustic waves by the "LD" scheme and test the convergence. We choose $\alpha = 1, \varepsilon = 0.1, \Delta x = 1/100, \Delta t = 1/1000$. Here Δt is chosen to stabilize the scheme and decreasing Δt alone will not improve much the numerical accuracy. Similar to Klein's paper [17], $P(\rho_\varepsilon)$ and the initial conditions are chosen as

$$P(\rho_\varepsilon) = \rho_\varepsilon^{1.4}, \qquad \qquad \text{for } x \in [-1, 1]$$
$$\rho_\varepsilon(x, 0) = 0.955 + \frac{\varepsilon}{2}\big(1 - \cos(2\pi x)\big), \quad u_\varepsilon(x, 0) = -\text{sign}(x)\sqrt{1.4}\big(1 - \cos(2\pi x)\big).$$

The initial density and momentum are displayed in Figure 5.

For $\varepsilon = 0.1$, the numerical results of the "LD" scheme at different times T are shown in Figure 6. The initial data approximate two acoustic pulses, one right-running and one left-running. They collide and their superposition gives rise to a maximum in the density. Then the pulses separate again. This procedure is demonstrated clearly in Figure 6.
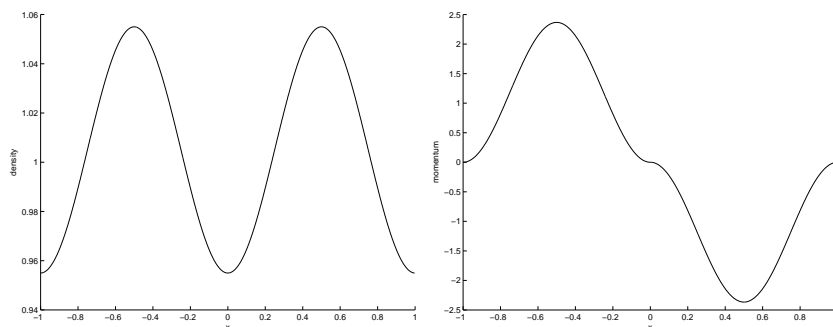
23

Figure 5: Example 2. When $\varepsilon = 0.1$, the initial density and momentum are displayed.

Example 3 In this example, we show numerical results for the two dimensional case. Let $P(\rho) = \rho^2$ and the computational domain be $(x, y) \in [0, 1] \times [0, 1]$. Because no shock will form in this example, we choose $\alpha = 0$ and the initial condition as follows:

$$\rho(x, y, 0) = 1 + \varepsilon^2 \sin^2(2\pi(x + y)),$$

$$\mathbf{q}_1(x, y, 0) = \sin(2\pi(x - y)) + \varepsilon^2 \sin(2\pi(x + y)),$$

$$\mathbf{q}_2(x, y, 0) = \sin(2\pi(x - y)) + \varepsilon^2 \cos(2\pi(x + y)).$$

The initial conditions for $\varepsilon = 0.8$ and numerical results at $T = 1$ calculated with $\Delta x = 1/20, \Delta t = 1/80$ are shown in Figure 7. Numerical tests show that a similar CFL condition is required as for the one-dimensional case. When $\varepsilon = 0.05$ at time $T = 1$, the numerical results with an unresolved mesh $\Delta x = 1/20, \Delta t = 1/80$ and a resolved mesh $\Delta x = 1/80, \Delta t = 1/320$ are displayed in Figure 8. We can see that the results using the coarse mesh are much 'smoother' than the one using the refined mesh. In this example the amplitude decay due to numerical diffusion cannot be ignored. When a coarse mesh is used, the first order method is known to have dissipation. This is mainly due to the numerical diffusion term, which smoothes out the solution. This phenomenon not only happens when ε is small but also when ε is $O(1)$. We can also see from Figure 8 that when ε is small, $D^x \mathbf{p}_{1\varepsilon} + D^y \mathbf{p}_{2\varepsilon}$ is close to 0.

As a comparison, the numerical solutions of the incompressible limit (4) with and without numerical viscosity are shown in Figure 9. The latter is obtained by a difference method based on a staggered grid configuration [13]. This staggered difference method is attractive for incompressible flows, since no artificial terms
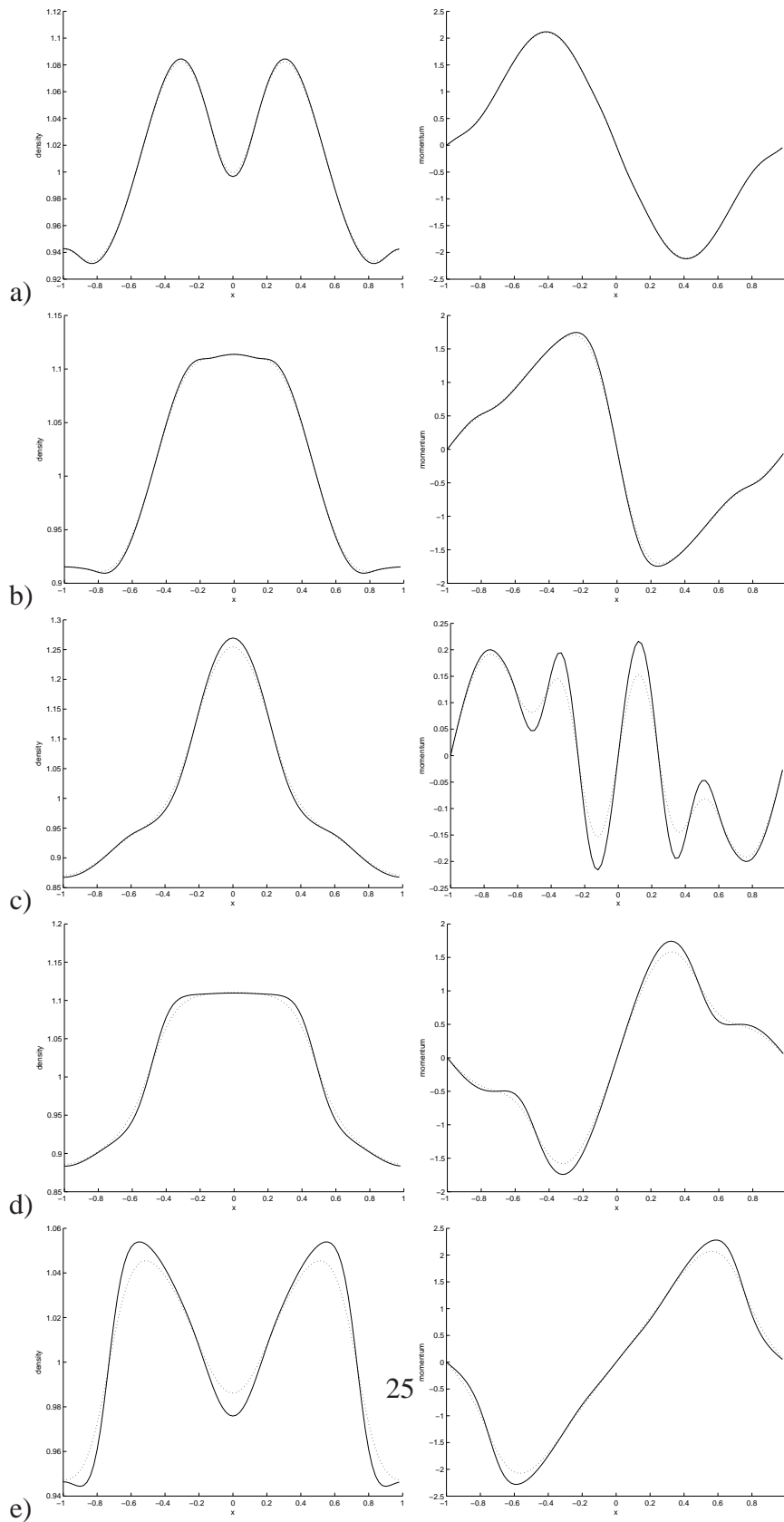
24

25

Figure 6: Example 2. When $\varepsilon = 0.1$, the density and momentum of the "LD" scheme at different times are represented: a) $T = 0.01$; b) $T = 0.02$; c) $T = 0.04$; d) $T = 0.06$. e) $T = 0.08$. All these pictures correspond to $\Delta x = 1/50, \Delta t = 1/1000$.

are needed to obtain stability and suppress the oscillations. Because of the stable pressure-velocity coupling, solutions with almost no viscosity can be obtained. The viscosity introduced here is of the form $\frac{A}{2}\Delta x$ where A is given by (36). We can see that the amplitude of the wave decays as time evolves even though the viscosity is only $O(\Delta x)$. In the limit of $\varepsilon \to 0$, (42) generates a discretization of the incompressible limit with $O(\Delta x)$ numerical diffusion terms. This is why the results for $\Delta x = 1/20, \Delta t = 1/80$ in Figure 8 are close to those with viscosity in Figure 9. When the meshes are refined, less diffusion is introduced and the solution becomes closer to the solution with no viscosity. The scheme indeed catches the incompressible Euler limit and good numerical approximations can be obtained without resolving ε, which confirms the AP property that is proved in section 4. However we need to take care of the numerical diffusion when coarse meshes are used. One possible way to improve this is to use less diffusive shock capturing schemes at first order or higher order schemes using the MUSCL strategy for instance [8, 19, 20], or to use staggered grid discretizations.

7   Conclusion

We propose an all speed scheme for the Isentropic Euler equation. The key idea is the semi-implicit time discretization, in which the low Mach number stiff pressure term is divided into two parts, one being treated explicitly and the other one implicitly. Moreover, the flux of the density equation is also treated implicitly. The parameter which tunes the explicit-implicit decomposition of the pressure term allows to suppress the nonphysical oscillations. The numerical results show that the oscillations around shocks of $O(\varepsilon^2)$ strength can be suppressed by choosing $\alpha = 1$. The low Mach number limit of the time semi-discrete scheme becomes an elliptic equation for the pressure term, so that the density becomes a constant when $\varepsilon \to 0$. In this way, the incompressible property is recovered in the limit $\varepsilon \to 0$. Implemented with proper space discretizations, we can propose an AP scheme which can capture the incompressible limit without the need for $\Delta t, \Delta x$ to resolve ε.

In this paper we demonstrate the potential of this idea by using the first order Lax-Friedrich scheme with local evaluation of the wave speeds. Though this first order method is quite dissipative, we can observe that the scheme is stable independently of ε and that the CFL condition is $\Delta t = O(\Delta x)$ uniformly in ε. It can also capture the right incompressible limit without resolving the mach number. Higher order space discretizations like the MUSCL method [8, 19, 20] can be built
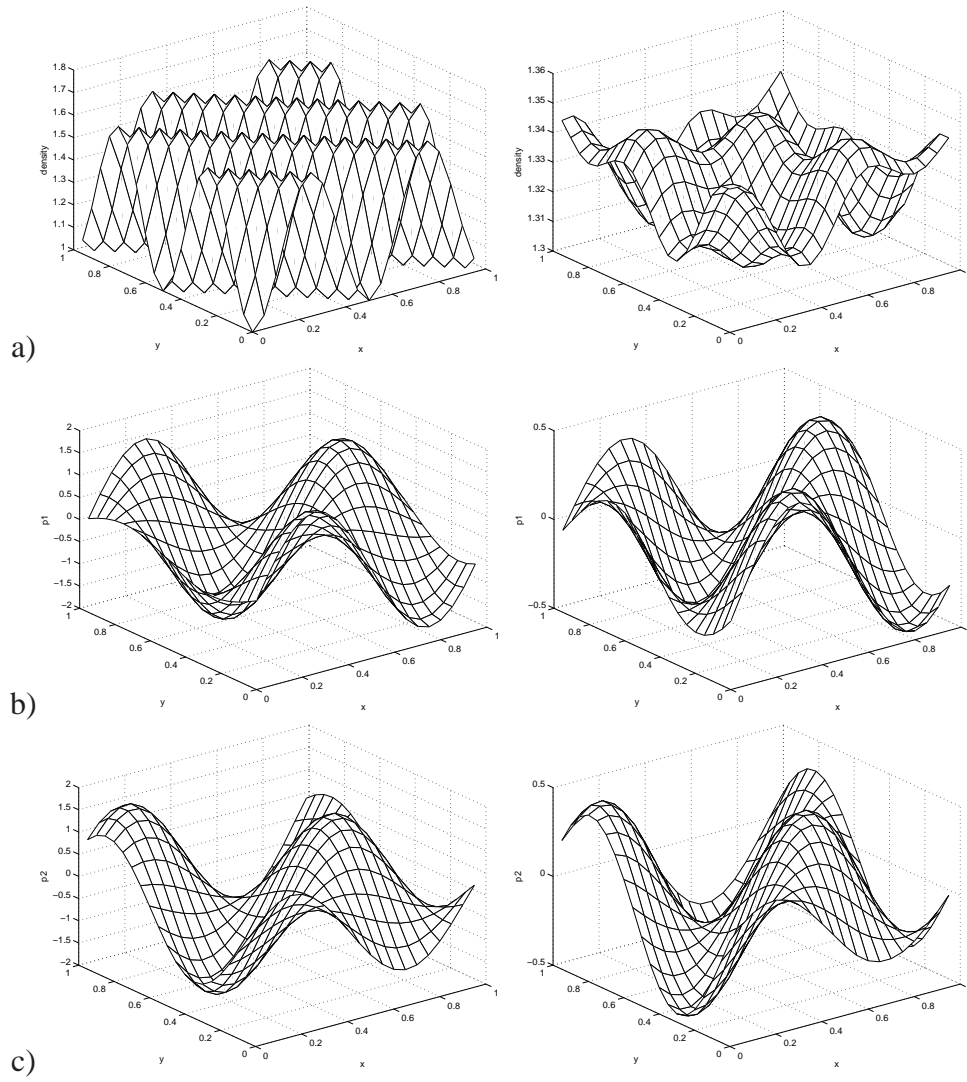
Figure 7: Example 3. When $\varepsilon = 0.8$, the initial density and momentum (left) and the numerical result with $\Delta x = 1/20, \Delta t = 1/80$ at time $T = 1$ (right) are represented. a) ρ_ε; b) $\mathbf{p}_{1\varepsilon}$; c) $\mathbf{p}_{2\varepsilon}$.
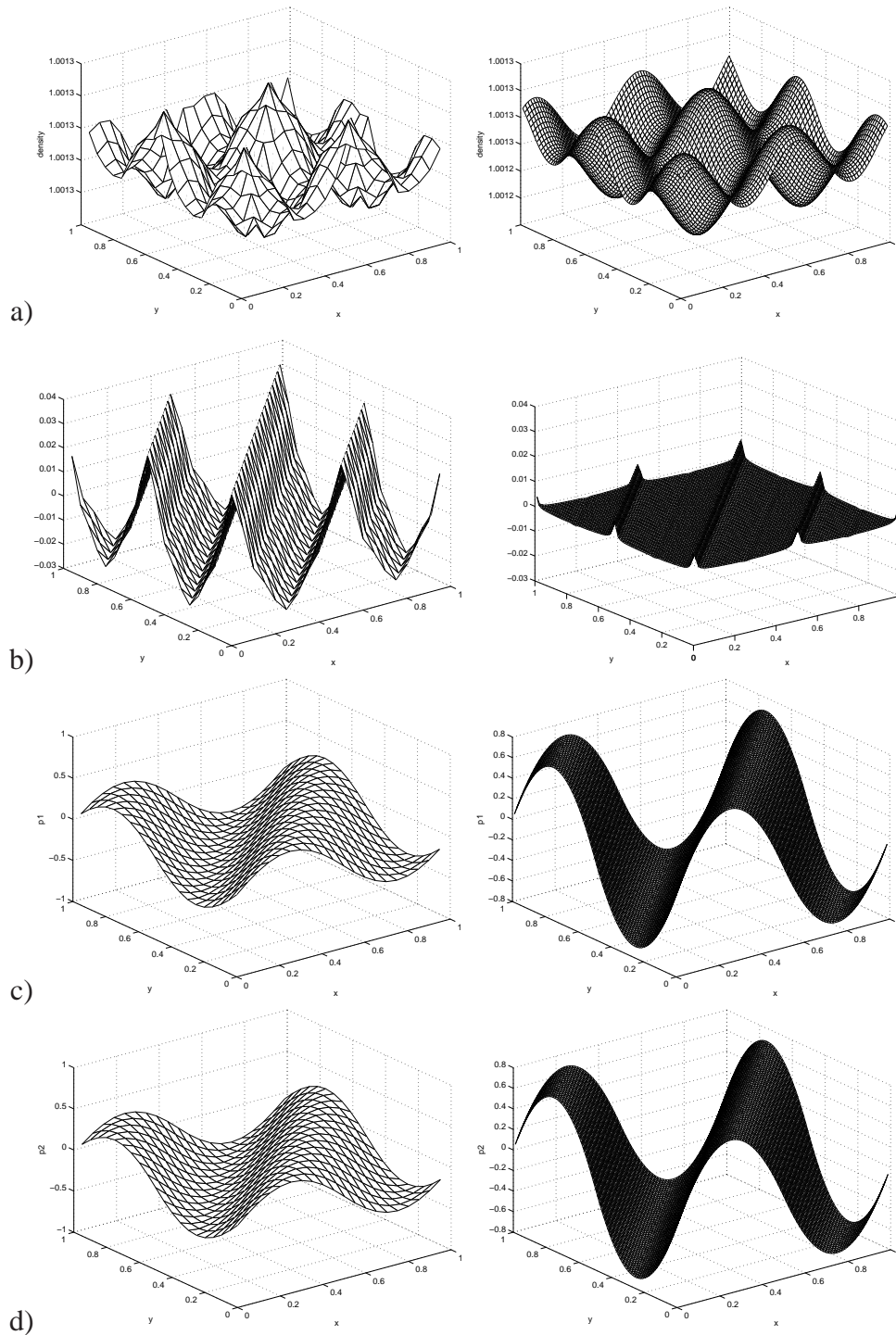
Figure 8: Example 3. When $\varepsilon = 0.05$, the numerical result with $\Delta x = 1/20, \Delta t = 1/80$ (left) and $\Delta x = 1/80, \Delta t = 1/320$ (right) at time $T = 1$ are represented respectively. a): ρ_ε; b): $D^x \mathbf{p}_{1\varepsilon} + D^y \mathbf{p}_{2\varepsilon}$; c): $\mathbf{p}_{1\varepsilon}$; d): $\mathbf{p}_{2\varepsilon}$.
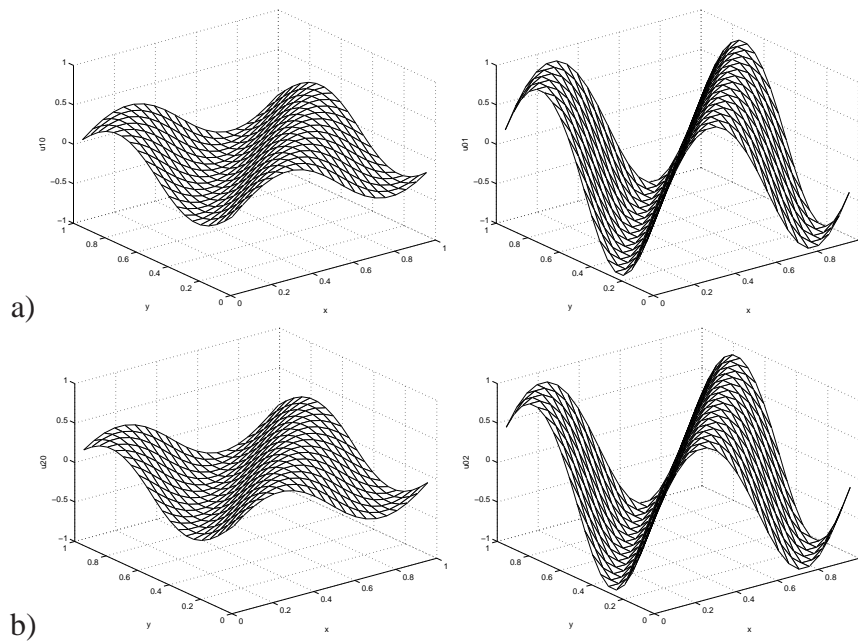
29

Figure 9: Example 3. The numerical results of the incompressible Euler limit using $\Delta x = 1/20, \Delta t = 1/80$ with (left) and without (right) viscosity at time $T = 1$ are represented. a): the first element of the velocity $\mathbf{u}_{01}$; b): the second element of the velocity $\mathbf{u}_{02}$.

into this framework. This is the subject of current work.

This paper provides a framework for the design of a class of all speed schemes. Compared with the ICE method [13, 12] and some recent work by Jin, Liu and Hauck [11], the idea is simpler and more natural. This framework can also be easily extended to the full Euler equation and flows with variable densities and temperatures. These extensions and applications [22] will be the subject of future work.

Acknowledgments

References

[1] H. Bijl, P. Wesseling, A unified method for computing incompressible and compressible flows in boundary-fitted coordinates, J. Comput. Phys., 141: 153-173, (1998)

[2] M. P. Bonner, Compressible subsonic flow on a staggered grid, Master thesis, The University of British Columbia. (2007)

[3] P. Constantin, On the Euler equations of incompressible fluids, Bulletin of the American Mathematical Society, Vol. 44, No. 4, 603-621, (2007)

[4] P. Crispel, P. Degond, M-H. Vignal, An asymptotic preserving scheme for the two-fluid Euler-Poisson model in the quasineutral limit, J. Comput. Phys., 223, 208-234, (2007)

[5] P. Degond, F. Deluzet, A. Sangam, M-H. Vignal, An asymptotic preserving scheme for the Euler equations in a strong magnetic field, J. Comput. Phys, Vol. 228, No.10, 3540-3558, (2009)

[6] P. Degond, S. Jin and J-G. Liu, Mach-number uniform asymptotic-preserving gauge schemes for compressible flows, Bulletin of the Institute of Mathematics, Academia Sinica, New Series, 2, No. 4, 851-892, (2007)

[7] P. Degond, J-G. Liu, M-H. Vignal, Analysis of an asymptotic preserving scheme for the Euler-Poison system in the quasineutral limit, SIAM J. Numer. Anal., 46, 1298-1322, (2008)

[8] P. Degond, P. F. Peyrard, G. Russo and P. Villedieu, Polynomial upwind schemes for hyperbolic systems, Partial Differential Equations, Series 1: 479-483, (1999)

[9] F. Golse, S. Jin and C.D. Levermore, The Convergence of Numerical Transfer Schemes in Diffusive Regimes I: The Discrete-Ordinate Method, SIAM J. Numer. Anal., 36, 1333-1369, (1999)

[10] J. R. Haack and C. D. Hauck, Oscillatory Behavior of Asymptotic-Preserving Splitting Methods for a Linear Model of Diffusive Relaxation, Los Alamos Report LA-UR 08-0571, to appear in Kinetic and Related Models, (2008)

[11] J. Haack, S. Jin and J. G. Liu, All speed asymptotic preserving schemes for compressible flows. in preparation.

[12] F. H. Harlow, and A. Amsden, A numerical fluid dynamics calculation method for all flow speeds, J. Comput. Phys, 8, 197-213, (1971)

[13] F. H. Harlow and J. E. Welch, Numerical calculation of time-dependent viscous incompressible flow of fluid with free surface, Phys. Fluid, 8, No.12, 2182-2189, (1965)

[14] R. I. Issa, A. D. Gosman, A. P. Watkins, The computation of compressible and incompressible flow of fluid with a free surface. Phys. Fluids, 8, 2182-2189, (1965)

[15] S. Klainerman, A. Majda, Singular limits of quasilinear hyperbolic systems with large parameters and the incompressible limit of compressible fluids, Communication on Pure and Applied Mathematics, 34: 481-524, (1981)

[16] S. Klainerman, A. Majda, Compressible and incompressible fluids, Communication on Pure and Applied Mathematics, 35: 629-653, (1982)

[17] R. Klein, Semi-implicit extension of a Godunov-type scheme based on low Mach number asymptotics I: one-dimensional flow, J. Comput. Phys. 121: 213-237, (1995)

31

[18] R. Klein, N. Botta, T. Schneider, C. D. Munz, S. Roller, A. Meister, L. Hoff-mann, T. Sonar, Asymptotic adaptive methods for multi-scale problems in fluid mechanics, J. Eng. Math., 83:261-343, (2001)

[19] A. Kurganov and E. Tadmor, New high-resolution central schemes for non-linear conservation laws and convection-diffusion equations, J. Comput. Phys., 160: 214-282,(2000)

[20] A. Kurganov and E. Tadmor Solution of two-dimensional Riemann problems for gas dynamics without Riemann problem solvers, Numerical Methods for Partial Differential Equations, 18:548-608,(2002)

[21] R. J. Leveque, Numerical methods for conservation laws, Lectures in Mathematics ETH Zrich, (1992)

[22] C. D. Munz, M. Dumbser and S. Roller, Linearized acoustic perturbation equations for low Mach number flow with variable density and temperature, J. Comput. Phys. 224: 352-364, (2007)

[23] C. D. Munz, S. Roller, R. Klein and K. J. Geratz. The extension of incompressible folw solvers to the weakly compressible regime, Comp. Fluid, 32: 173-196, (2002)

[24] J. H. Park and C. D. Munz, Multiple pressure variables methods for fluid flow at all Mach numbers ,Int. J. Numer. Meth. Fluid, 49: 905-931, (2005)

[25] S. V. Patankar, Numerical heat transfer and fluid flow, New York: McGraw-Hill, (1980)

[26] F. Rieper and G. Bader, The influence of cell geometry on the accuracy of upwind schemes in the low mach number regime, J. Comput. Phys., 228: 2918-2933, (2009)

[27] D. R. van der Heul, C. Vuik and P. Wesseling, A conservative pressure-correction method for flow at all speeds, Comptuers and Fluids, 32, 1113-1132, (2003)